Effects of grouting in reducing excessive tunnel lining deformation: Field experiment and numerical modelling using material point method

Effects of Grouting in Reducing Excessive Tunnel Lining Deformation: Field Experiment and Numerical Modelling using Material Point Method

Tianchi Zhao[a,f], Tianran Han[b,c,*], Gang Wu[b,c], Yong Gao[d], Yong Lu[e]

[a] Department of Geotechnical Engineering, College of Civil Engineering, Tongji University, Shanghai 200092, China

[b] Key Laboratory of Concrete and Prestressed Concrete Structures of the Ministry of Education, Southeast University, Nanjing 211189, China

[c] National and Local Joint Engineering Research Center for Intelligent Construction and Maintenance, Nanjing 211189, China

[d] Nanjing Metro Operation Co., Ltd, Nanjing 210046, China

[e] Institute for Infrastructure and Environment, School of Engineering, The University of Edinburgh, Edinburgh EH9 3JL, UK

[f] Shanghai Investment and Consulting Corporation, Shanghai 200001, China

* Corresponding author: Tianran Han, No.2 SEU Road, Nanjing, China, 211189; Email, tianran.han@hotmail.com; Phone, +8615905168891

Acknowledgement

The authors would like to acknowledge the financial support provided by the National Natural Science Foundation of China (Grant No. 51525801) and the China Scholarship Council (Grant No. 201806260197 and No. 201706090072).

Abstract

Excessive deformation of tunnel lining structures can be identified as a common problem in Eastern China soft ground. Grouting treatment is an effective and common method to actively mitigate excessive cross-sectional deformation of tunnel lining rings in soft soils. However, grouting operations would introduce localized heavy disturbance to the surrounding ground around the grouting nozzles, causing large-deformational soil movement. The occurrence of large soil movement makes it difficult to use traditional finite element methodologies when it comes to modeling the effects of the grouting treatment on tunnel lining structures. To cope with this challenge, this paper proposes a simulation framework based on the Material Point Method, which enables explicit modeling of the grouting injection process and natural incorporation of large deformation. On the other hand, a field experimental study of an operational shield metro tunnel with grouting treatment has been conducted. The experimental study involved an extensive monitoring scheme and various geometrical arrangements of the grouting operation, thus the data from the field monitoring records enable a comprehensive comparison with the numerical results. The comparison between the experimental and numerically simulated results from the grouting treatment shows a satisfactory agreement. A sensitivity analysis of the grouting parameters is then carried out. The results from both the field experiment and numerical simulation show that with the

increase of the height and volume of the grout, the recovery effect of the horizontal convergence is improved. However, limiting values of these grout parameters exist, beyond which any further increase would become less effective. The relative positions of the grouting to the tunnel, both horizontally and vertically, also show a sensitive effect.

Keywords: tunnel lining's deformation, shield tunnel, grouting, numerical simulation, material point method, sensitivity analysis

Highlights

- A field experiment of grouting treatment was conducted to study the grouting effects on tunnel linings.
- Material point method was used to explicitly model the grouting injection, considering large-deformational soil movement naturally.
- Effects of key grouting parameters were studied through a sensitive analysis to optimize grouting design.

1. Introduction

Shield tunnel structures built in soft grounds are often found to suffer from problems of over-deformation with excessive convergence, due to the low resistance of the surrounding soil against the cross-sectional diametrical expansion of lining rings. The existing deformation could be further enlarged due to adjacent construction-related soil movements, such as deep excavations or unexpected surcharges. In some cases in Eastern China soft ground, the convergence was found to almost reach the level corresponding to the ultimate bearing capacity of segmental linings (Wang, 2009; Huang et al., 2017).

Large convergence can lead to potential structural problems like cracking, spalling, and leakages. Therefore, adequate control measures are vital for the safety of tunnel structures. In recent years, researchers have developed several methods to solve this kind of problems in engineering practice, such as using steel ring reinforcement (Kiriyama et al., 2005), polyester patching reinforcement (Banthia, 2013) and grouting-based approaches (Ding et al., 2019). Unlike the reinforcement-type passive deformation control methods, grouting-based treatment methods introduce active control mechanisms enabling recovery of the over-deformed lining rings to an acceptable level. During the grouting treatment, fast-setting grout is injected into the soil, generating a soil-concrete mixture with enhanced ground resistance to the developing lining expansion movements. In the meantime, the treatment also introduces counter-pressure against the unbalanced pressure released by adjacent engineering activities. Successful applications of this procedure have been reported from several grouting projects, especially in soft soil areas like the Eastern China soft ground (Xie et al., 2007, Zhang et al.,2010).

The effect of grouting can be better understood through suitable theoretical methodologies, in-

situ, and mock-up experiments. Several analytical solutions have been developed to describe the evolution of grouting behaviors, especially the grouting pressure (e.g. Ye et al, 2009). These theoretical formulations involve simplified assumptions such as constant grouting and flow parameters (stress, velocity, and volume) and do not take into account the complexities that can often arise in real engineering conditions. Therefore, these solutions can find themselves difficult to apply for complex projects. Moreover, to obtain the key parameters used in these simplified solutions, the field monitoring would generally be required (Harris et al., 1994, Bezuijen et al., 2004). Since field measurement works are understandably restricted to specific conditions of a given project, some mock-up experiments have been conducted in the grouting research studies (Bolton, 1996; Ding et al., 2019; Zhao et al., 2019) to replicate various situations and extend the validation of parameters in the corresponding theoretical equations. However, such experimental exercises can be costly and also time-consuming.

Considering the limitations of the analytical and experimental methodologies, numerical methods tend to provide a more versatile means to simulate the grouting process and its effects under realistic soil and tunnel structural conditions. Traditional finite element analysis (FEA) has been widely used in grouting project modeling. In the FEA framework, grouting is commonly simulated by applying internal pressure to the corresponding elements in the grouted region. Specifically, in some studies, this internal pressure is loaded onto the zero-thickness embedded interface elements (Wisser et al., 2005; Lambrughi et al., 2012; Oh and Ziegler, 2014; Liu et al., 2016), and in some other studies it is loaded onto the grout layer elements (Soga et al., 1999; Kasper and Meschke, 2006; Katebi et al., 2015). It is clear that under such FEA framework the material injection process of grouting is not represented explicitly, and instead, the grouting-induced pressure is exerted to the surrounding soil with approximate pressure evolution. Therefore, the complex interaction between the grouting operation and the soil is largely missing. As a matter of fact, the grout injection with a high pressure usually involves large localized ground deformation around the grouting nozzles; it is difficult for mesh-based methods like FEM to model adequately such large deformation effects due to elemental-distortion related issues.

As a new generation mesh-free numerical method, Material Point Method (MPM) is free from the above limitations, and is therefore inherently more suitable to simulate this problem. The MPM is one of the latest and popular developments in Particle in Cell (PIC) methods (Nguyen, 2014). Originally developed for hydrodynamic problems, it is currently growing in its popularity in solving solid mechanics problems (Richefeu and Villard, 2016), especially those involving large deformations such as excavations (Cheng et al., 2015, Fern, 2019), footing strips (Woo and Salgado, 2018) and slope failures (Wang, 2016). The MPM discretizes the objects being modeled into a series of material particles, which carry with them all state variables including mass, velocity, strain, stress, etc. A particular material subdomain is also assumed to concentrate on the corresponding particles. The computation procedure of the MPM is schematically illustrated in Fig.1. Details of the MPM formulations can be found in the relevant literature (Sulsky, 1994; Fern, 2019).

This paper proposes a detailed modeling workflow to simulate the grouting treatment operations for shield tunnel projects based on the MPM, enabling explicit modeling of the injection process and therefore, the detailed grouting procedures. On the other hand, a full-scale grouting treatment field experiment has been carried out in Eastern China soft ground. The experiment provides first-hand field data for an analysis of the effects of a varying arrangement of the grouting on the reduction of the existing convergence, and the experimental data also enables validation and comparison for the proposed numerical modeling scheme. Detailed simulation results and monitoring records of lining ring deformational behaviors under grouting operations are compared and discussed. A systematic parametric study is subsequently carried out to investigate the effects of variations of the grouting parameters, such as relative positions, grouting height, and grouting volume. On this basis, recommendations are made for the design of grouting operations in engineering practice.

2. Tunnel lining grouting treatment and field monitoring

2.1. Excavation-induced large tunnel deformation

2.1.1 Background

Recent years have seen a rapid expansion of metro systems in big cities in China as an effective means to increase urban transportation capacities and ease the pressure of traffic congestions. This also tends to incentivize the further expansion of the city itself, bringing more buildings to be constructed along the metro corridors. As a result, more engineering activities take place in close proximity to the metro tunnels, generating potential problems to the tunnel structures (Li et al., 2016, Hu et al., 2003). Engineering activities like deep excavations, surcharges, or tunneling introduce additional deformation to the existing tunnel structures, which can adversely affect the safety of the tunnel. For soft ground cases, the deformational problem is known to be particularly significant (Wang, 2009; Huang et al., 2017; Ding and Xu, 2017).

In this section, we will examine a case where a section of a shield metro tunnel was heavily disrupted by nearby large deep excavations. The disrupted section of the tunnel is situated in the soft ground in a newly developed urban region in Nanjing, China. The excavations led to excessive cross-sectional deformation of the tunnel, and active mitigation measures using grouting treatment were subsequently introduced to retrofit the tunnel lining structures.

The tunnel sections were bored by earth pressure balanced tunneling machines and subsequently put into service in 2010. After 2 years of operation, deep large excavations started close to both sides of the twin tunnels as part of a development project for a financial center consisting of 10 high-rise buildings. Fig. 2a shows a plan view of the construction sites. The whole excavation site was divided into four zones. The excavation in the zone I and zone III were deemed to be the main reason causing the tunnel offloading effect, so herein we focus our attention on the excavation in these two zones.

2.1.2 Soil properties

The geology of this region features a typical Nanjing soft deposit characterized by layered formations. The stratum mainly consists of the made ground, silty clay, and fine sand. Thick muddy silty clay constitutes a great proportion of the upper stratum and forms the major weak layer of the deposits, which is characterized by low permeability, high water contents, and low resistance to tunnel diametrical expansion. Beneath the muddy silty clay, the fine sand is another major thick deposit, overlaying coarse sand and weathered mudstone. Fig. 2b**Error! Reference source not found.** shows the spatial relationship between the twin tunnels to the excavation zone I and zone III, and the representative cross-sectional geological profile of the soil formation at the grouting testing site, which is extracted from borehole data.

2.1.3 Lining structures

Fig.3a**Error! Reference source not found.** shows the typical tunnel lining design. The lining ring is staggered-joint assembled by 6 prefabricated RC segments with an outer diameter of 6.2 m, a width of 1.2 m, and a thickness of 0.35 m. Adjacent segments are connected with two M30 curved steel bolts with a strength of 400 MPa. As a reference, the maximum convergence of these linings immediately after the completion of the tunneling stage was about 0.2%D (D is the outer diameter of the tunnel), which was within an acceptable range. No obvious fast-evolving development of the deformation was observed before the start of the nearby excavations. As such, the initial deformation after the completion of the tunneling is deemed to have no influence on the large convergence problem due to the excavations.

2.1.4 Tunneling procedures

The excavation in the zone I was initiated in Feb. 2012 and completed by bottom concrete slab casting in Jul. 2013. The whole substructure of zone I was completed in Nov. 2013. Excavation in zone III followed right after the completion of the bottom slab casting in the zone I in Jul. 2013. By Oct. 2013, the impacts from the excavations were found to be quite substantial for the cross-sectional response of the tunnels. As shown in Fig.4, about 300 rings (ring number 460 to 760) in the left line tunnel were heavily affected by the deep excavations, with the convergence-to-diameter ratio, $\delta D/D$, being greater than 0.5%. In particular, rings 508 to 666 corresponding to zone I were most affected and the $\delta D/D$ ratio ranged from 1.02% to 1.40%, far beyond the relevant design regulation (MOHURD, 2014).

To ensure the safe operation of the metro line, it was decided to address the issue using grouting treatment on both sides of the deformed tunnel (left line) to push the tunnel shape back to an acceptable deformation level and improve soil resistance. This method has been proven effective to tackle similar problems in Shanghai (Zhang et al., 2018). However, the engineering experience of using the grouting technique was limited for the specific geological condition in Nanjing at that time. Therefore, a field grouting experiment on some selected rings (rings 580 to 588 of the left line in Fig.4) were conducted first before the implementation of the technique on a larger scale, in the hope to optimize the grouting parameters for the specific engineering practice.

The experiment was conducted from Oct. 30, 2013 to Nov. 10, 2013. It is worth noting that as the grouting experiments were being conducted, the excavation activities in the zone I had already finished, while excavation in zone III was in progress at its 3rd level and its effect on the left line tunnel was expected to be insignificant due to the relatively large distance. Therefore it is reasonable to ignore any incremental deformation due to excavation in the evaluation of the effects of the grouting experiments, which will be presented in later sections.

2.2. Grouting treatment in the experiment

2.2.1 General introduction

Fig.5 presents the grouting system and working procedures. The basic idea was to create grouting conductors from the ground and inject grout to the designed location near the tunnel. Before the operation, accurate tunnel position was measured in terms of coordinates of tunnel outer side faces and its burial depth. After this, holes were drilled according to the design to a depth of the tunnel crown elevation. To maintain the integrity of the holes, casing pipes of similar diameter as the drilled holes were installed inside the holes to prevent soil cave-in and facilitate an easy installation for grouting pipes. Afterward, a grouting pipe was driven inside the casing pipe until its lower end reached the tunnel heel elevation. The grouting injection system was then assembled by connecting grouting pumps, flow meter, grouting mixer to the grouting pipes. The grouting injection system was checked to make sure it was unobstructed before the actual grouting operation. After the injection system was put in place, cement slurry and water glass were prepared. The grouting was conducted using two separate pumps, each responsible for the injection of cement slurry and water glass, respectively. The two liquids were mixed and injected into the grouting pipe through a grouting mixer and monitored in real-time for the liquid flow rate by a flow meter.

The grouting was conducted in a manner to minimize its disturbance to the surrounding soil. Specifically, the grouting pipe was lifted upwards at a steady speed using a special pipe-lifting device as the grout-injection carried on, and the grout-injection was done slowly and steadily. After the grouting procedure was completed and the grouting pipe was lifted to the lower end of the casing pipe, the grouting pipe was kept still for about 10 minutes to allow for the initial settling of the grouting materials. After this, the entire grouting pipe was lifted out from the ground by the pipe lifting device to complete the grouting operation for one hole.

2.2.2 The geometry of the grouting process

Four different locations (A1, A2, B1, and B2 in Fig.5) were designed for the installation of grouting tubes in different cases, which were symmetrically located to the center of the tunnel cross-section, with A2 and B1 being closer to the tunnel. The total height of the grouting zone was set as 5.2 m originally, and the elevation of its bottom end is identical to that of the bottom of the lining rings. However, the grouting positions from Oct. 30 to Nov. 6 were 2.7 m higher than the original design (Position "I" in Fig.5), and this was caused by a mismeasurement of the tunnel's depth. Additionally, the total height of the grouting zone on Nov. 7 was adjusted to 4.2 m (Position "II" in Fig.5). These changes would have caused some deviation from the expected results, nevertheless,

they should not affect the comparison with the numerical modeling and the variation in the positions provides a diverse range of comparison cases.

2.2.3 Working schedule and grouting parameters

The grouting treatment was implemented to the rings Z580~Z588 in the left line tunnel. Fig.6 presents the detailed daily working schedule from Oct. 30, 2013 to Nov. 10, 2013. Four colored cubes are used as the representation for different grouting positions (A1, A2, B1, and B2), while gray cubes indicate the existing grout injections. Total grouting volumes unit in liter are also shown for new grout injections each day. The grouting control parameters were determined empirically and the details are given in Table. 1.

Table. 1 Empirical grouting control parameters

Grouting pressure p_g /MPa	Total area of grouting holes A_g / m^2	Grouting flow rate Q / $L \cdot \min^{-1}$		Grouting velocity v_g / m·s^{-1}
		Cement slurry	Water glass	
1.0	1×10^{-4}	14~16	5~10	4.2

2.3 Field monitoring

Automatic field monitoring was conducted to obtain the deformational response of the tunnel and provide information for safety assurance and potential plan adjustment of the grouting operations. Considering that the main objective of the grouting operation was to restore the ovalized tunnel cross-sections towards the original circular shape, the horizontal convergence of the tunnel was used as the main indicator to evaluate the deformation response. Leica TM30 robotic total stations and reflection prisms, which were placed on the tunnel inner surface at its spring line, were used for the deformation monitoring of the lining rings during the grouting experiment (Fig.3b**Error! Reference source not found.**). The accuracy of the monitoring system was calibrated to be smaller than ±0.5 mm. Considering the requirements to achieve acceptable accuracy, the intervals between two total stations were set to be no greater than 60 meters. In this way, all rings in the excavation-affected zone were properly covered.

The monitoring system enabled the rapid acquisition of the deformation response at intended time intervals. In the grouting experiment data acquisition, intervals were set at every 5 or 10 minutes, according to the field-observed convergence changing rates. During the testing, the real-time monitoring data were gathered and passed on to the grouting team to guide their grouting operations. In the meantime, structural damages in terms of cracking, spalling, or leakages were also closely inspected and monitored as the grouting operations were undergoing. Referring to the related engineering experiences from Shanghai practice (Liao et al., 2009), warnings were issued to the grouting team if convergence response exceeded 1 mm or minor structural damages were found during the grouting operation, while immediate stop of the operation was required if convergence change exceeded 5 mm, or significant structural damages were spotted.

2.4 Data analysis

2.4.1 Total convergence

The total station started acquiring data on Oct. 30, 2013 and provided the evolution of the horizontal convergence at the middle cross-section of the grouting-treated lining rings from Z581 to Z589. Data were acquired during the grouting-treatment stage (Oct. 30, 2013 to Nov. 10, 2013) and the after-grouting stage (Nov. 11, 2013 to Dec. 7, 2013). Fig.7a shows the measured horizontal convergence over the above two periods. It can be seen that the evolutions from different rings share a similar trend consisting of a descending period during the grouting process, and an ascending period after the completion of grouting. The excess pressure generated tends to rupture the soil surrounding the grouting nozzles, inducing a directional thrust onto the tunnel and thus pushing the tunnel to retreat to a smaller convergence. Thereafter, due to the process of excess pore pressure dissipation and the solidification of grout, the deformation recovery could not be maintained fully and a certain amount of rebound occurred. Therefore, two phases of deformational response could be identified, namely a recovery phase and a rebound phase, as follows:

(i) Recovery phase: In this phase, the total convergence was reduced by about 15 mm in each ring, which was about 20% of the original value. As no grouting treatment was exerted for Ring 588-589 directly, the reduction of convergences was smaller here than in other rings.

(ii) Rebound phase: The rebound started following the termination of the grouting treatment, and lasted for about 20 days The rebound in the first 10 days accounts for about 80% of the total rebound value and finally led to a loss of about 35% of the recovery convergence by grouting.

The rebound phase is influenced by multiple factors such as the permeability of the soil and the properties of the grout, and an in-depth discussion on these factors is out of the scope of this paper. It is interesting to note that the total rebound value appears to exhibit a linear relationship with the initial reduction of the convergence from grouting, as shown in Fig.7b, and this observation suggests that the rebound value may be estimated in proportion to the recovery results. In this respect, we shall focus on the under-grouting process and study the immediate effect of grouting on the deformation of the linings in the context of large deformation problems.

2.4.2 Details of grouting effect

To study the grouting results of each single grouting treatment, the change of horizontal convergence from each procedure is calculated by the difference between the values of total convergence before and after grouting in a single day, and the results are shown in Fig.8. The effect of grouting on the convergence of individual rings tends to diminish very quickly with increased distance. The curves are presented in four groups based on the positions to demonstrate the convergence evolution more clearly.

According to the grouting schedule (Fig.6), only the work on Nov. 1 included multi-grouting procedures at the same ring, hence the resulting reduction of convergence is almost two times of other treatments. The results of Nov. 3 and Nov. 5 also proved that it was more efficient if the grout injections came from both sides of the tunnel simultaneously, as better results were also obtained in

these cases which had the second smallest longitudinal distance of two grouting treatments.

The grouting positions from Oct. 30 to Nov. 6 were higher than the original design. Monitoring data corresponding to these dates appeared to illustrate a more effective deformational control in terms of convergence recovery rate, as grouting occurred around the mid-height of the tunnel instead of at its heel.

The above field data indicates that the grouting position and grouting height are vital for the determination of the grouting efficiency. The grout volume is also expected to be an important influencing parameter but this could not be observed from the monitoring results as the grout volume remained similar in different cases. In the following simulation framework, we shall mainly focus on the investigation of these key parameters.

3 MPM framework

3.1 General information

Field experiments can provide first-hand information about the grouting effect on the tunnel convergence control. However, it is not possible to rely on such experiments to cover varying operation conditions and optimize the design parameters. In this regard, sound numerical simulation can play an important role. Here we choose the material point method for the numerical simulation as this method is particularly suitable to solve large deformation cases, making it possible to replicate the diffusion process of the grouting and incorporate the grouting-induced large deformational response of the ground in the simulation in a realistic manner.

As discussed in Section 2, the monitoring data suggests that the grouting effect on the deformation of the tunnel structure can largely be represented by the cross-sectional behavior of the tunnel, with the longitudinal behavior only being a secondary factor. Therefore, a 2D plane-strain MPM model is adopted to simulate the grouting treatment studied in Section 2. A total stress analysis is introduced, as the grouting procedure was conducted in the ground with low permeability, and the short-term behavior is focused.

The geometry of the model domain is assigned based on the actual conditions, as shown in Fig.9. The distances between the numerical boundaries to the closest tunnel are made larger than three times of the tunnel diameter to minimize the boundary effect, as suggested in a previous empirical simulation (Azúa et al., 2018). The bottom side of the model is fully fixed and the horizontal movements of the left and right sides are restrained as boundary conditions. Considering both the calculation accuracy and the computational efficiency, the background mesh element is defined as 0.5 m × 0.5 m. Each element consists of 4 particles (2 × 2), which means that the distance between two adjacent particles is initially 0.25 m. In total 20200 elements and 80000 particles are created at the initial status.

Two different interaction mechanisms between the grouting and the surrounding soil can be identified, namely the compensation (or compaction) effect and the fracturing effect (Mair and Hight, 1993), and they are controlled by the injection volume, property of soil, and viscosity of the grout.

The standard MPM is capable of replicating the compensation effect but not fracturing. Considering that the main effect that grouting exerts on the soil in the current case is through compensation, the fracture behavior is neglected here.

3.2 Simulation of grouting

The entire simulation includes three necessary processes: (i) stress field initialization, (ii) tunneling excavation, and (iii) grouting treatment. The initial stresses are calculated by K_0 method, defined as $K_0 = 1 - \sin\phi$, where ϕ is the friction angle of the soil. Some stabilized steps are needed to reach the equilibrium status and get a steady stress field under gravity.

The creation of the twin tunnels is firstly simulated by removing the particles within the tunnel area according to the geometry of the tunnels, and particles at the position of linings are assigned as the tunnel lining material to model the tunnel structures, and then followed by stabilization steps as well.

After the tunneling excavation, the model then introduces the grouting procedure. As the MPM is a particle-based method, new particles can be added into the system easily at specified positions and in a continuous manner to mimic the injection of grouting (Fig.9), which carries corresponding mass, stresses, and velocities. In this way, the grouting process is simulated in a more straightforward and direct manner. The main principle for the simulation is to maintain the mass and momentum conservations. Therefore, the total mass of all new grout particles should be equal to the actual grouting mass in each case, and their initial velocities are also defined according to the values listed in Table. 1.

As the grouting is implemented from the bottom and moves up with a constant velocity, ten points are arranged along the grouting zone uniformly in the MPM model as control positions for the addition of new particles. The grouting is then implemented at these positions one after another (Fig.9). 5 50 particles are added in each point continuously to keep a uniform grouting work, and the initial volumes of particles are computed according to the total injection volume and the number of new particles.

To focus on studying the grouting behavior along the cross-sectional direction, four representative cases from the experiment, in which the grouting treatment was only implemented in a single ring, are adopted in the simulation. The corresponding parameters are shown in Table 2.

Table 2 Grouting parameters in MPM model

Case	Date	Grouting parameters			
		Coordinates (Bottom) position / m	Ring	Position	Height / m
1	10-30	(48.1, 24.6)	Z587	B1	5.2
2	11-01	(35.9, 24.6)	Z580	A2	5.2
		(48.7, 24.6)	Z580	B2	5.2
3	11-07	(35.9, 21.9)	Z582	A2	4.2
4	11-10	(48.1, 21.9)	Z584	B1	5.2

3.3 Material properties

The linings and grout are assigned as simple elastic models(LE), and the grout is considered as being in an almost incompressible flow state with a low elastic modulus. Each soil layer is assumed to be isotropic and homogeneous. As the model is based on the total stress and undrained approach, the soil properties are defined using Tresca model (TR) following the standard method in geotechnical simulation, with cohesion set equal to the shear strength (s_u) of the corresponding soil layer. The Poisson's ratio should be set as 0.5 to represent the undrained condition (Artola, J, 2005). In the numerical model, a value of 0.45 is actually used to avoid the instability in the numerical computation, which can be caused by an extremely large bulk modulus when the Poisson's ratio gets close to 0.5. The other parameters are defined based on the data from the site investigation as shown in Table 3.

Table 3 Material parameters of the MPM model

Type	Constitutive model	Material parameters			
		Density ρ(kg/m^3)	Young's modulus E(kPa)	Poisson's ratio ν	s_u(kPa)
Tunnel lining	LE	2551	20000000	0.3	-
Grout	LE	2000	300	0.45	-
Fill	TR	1850	3270	0.45	13.0
Silty clay	TR	1790	2790	0.45	12.0
Fine sand	TR	1920	9830	0.45	34.5

3.4 Numerical results

Fig.10 presents the contours of the horizontal displacement caused by grouting. The compensation result can be observed with a semi-elliptic influence zone extended from the grouting zone; although the initial velocities of the grout particles are directed towards the left tunnel side, the compression effect is almost symmetric in Case-1, Case-3, and Case-4, which means the key factor that controls the grouting result is the pressure but not velocity. The local excess deformation in the soil can go up to 50 mm and leads to a 35 mm movement on the tunnel lining.

For Case-1 and Case-4, the main difference in the simulation is the elevation of the grouting positions. Case-1 has a higher elevation and the grouting is implemented in the soft clay layer, while the grouting in Case-4 is close to the lower stiffer sand layer, so the deformation is limited. Therefore the grouting will be more effective if it is carried out in a soft layer, and this is expected as the main mechanism is through compression and injection, which was also observed from the monitoring data. Besides, the simulation shows that the grouting volume also affects the result, and more grouting volume leads to a larger excess deformation. As Case-3 uses the lowest grouting position and a less grouting volume, the deformation caused by grouting is therefore the smallest.

When the compensation grouting is implemented on both lateral sides of the tunnel (Case-2), it can be seen that the result is similar to a combination of two one-side grouting operations. The

compression effect is enhanced and forms a larger influence zone. Besides, the symmetrical grouting on both sides of the left tunnel ensures a recovery of the convergence deformation of the tunnel without introducing a global disturbance (shift) of the central position of the tunnel. To investigate the effect of grouting sequence, a contrast case is also studied here, in which the grouting is carried out on both lateral sides simultaneously, and the other parameters are the same as the Case-2. Almost the same effect zone and recovery results are observed in this specific case. This confirms the above point about the result of the two-side grouting operation in that there is no obvious effect from the grouting sequence.

It should be noted that, although a grouting-induced large excess deformation is observed in the soil, the effective reduction of the lining convergence is much less than the total displacement. To compare the numerical results with the data from the field experiment, the developments of the displacements during the grouting treatment are plotted versus the current grouting volume in Fig.11.

The reduction in convergence is about 4 ~ 5 mm for the one-sided grouting (Case-1 and Case-4) and increases to 10 mm for the two-sided case (Case-2). The recovery in the Case-3 is only about 3 ~ 4 mm due to the lower grouting volume and elevation. The numerical results show good agreement with the field data, and this validates the accuracy of the MPM model.

The diagrams in Fig.11 suggest that there is a critical grouting volume in each of the four cases, such that the convergence reduction effect will markedly decrease after the grouting volume exceeds this value. This value is related to the soil properties and other grouting parameters. It is reasonable that the soil at the other side of the tunnel (opposite to the grouting side) needs to supply enough resistance to get an effective reduction on the convergence. As the two-sided grouting (Case 2) can enhance the resistance of both sides, hence it increases the critical grouting volume, resulting in a greater effect in the reduction of the convergence.

4 Sensitivity analysis

The field data and the numerical results all indicate that the efficiency of the grouting in reducing tunnel convergence is controlled by several key factors, and from the operational aspect these include the position, height, and volume of the grouting. Therefore, a detailed sensitivity analysis is useful to provide further insight into the influence trend of these factors and how optimized options may be obtained. For this purpose, the MPM model presented in Section 3 is employed to carry out a parametric study. In each parameter group, one of the original cases listed in Table 2, which has been validated by the monitoring data, is set as a benchmark for the comparisons.

4.1 Grouting position

The sensitivity analysis on the grouting positions involves two aspects, namely the horizontal position (A1, A2, B1, and B2 in Fig.5) and the vertical elevation (h1~h4, from 0 m to 2.7 m for the grouting start point relative to the bottom of lining). The experimental Case-1 is set as the benchmark to define all other parameters except the grouting position, with a height equal to 5.2 m, volume equal to 1593 L, and initial stress equal to 1000 kPa. Considering practicality, 16

comparative cases are defined and divided into two groups for variable horizontal and vertical directions, respectively. The details of the 16 cases are summarized in Table 4, and the detailed grouting zone of different cases can be seen in Fig.12. Note that the case numbers start from 5 here as cases 1~4 have been designated for the experimental cases. Furthermore, the elevations of Case-5 and Case-9 are the same as the cases in Group-2, so these two cases can also be included as comparison cases in the examination of horizontal grouting positions.

Table 4 Grouting parameters for sensitivity analysis of grouting positions

With different vertical positions (Group-1)			With different horizontal positions (Group-2)		
Case-Num	Start position	Grouting pipe	Case-Num	Start position	Grouting pipe
5	h1(35.3, 21.9)	A1	12	(37.0, 21.9)	A3
6	h2(35.3, 23.9)	A1	13	(35.9, 21.9)	A2
7	h3(35.3, 24.6)	A1	14	(34.0, 21.9)	A4
8	h4(35.3, 25.9)	A1	15	(32.0, 21.9)	A5
9	h1(48.1, 21.9)	B1	16	(47.0, 21.9)	B2
10	h2(48.1, 23.9)	B1	17	(48.7, 21.9)	B3
1	h3(48.1, 24.6)	B1	18	(50.0, 21.9)	B4
11	h4(48.1, 25.9)	B1	19	(52.0, 21.9)	B5

Fig.13a presents the total horizontal displacements of left and right boundaries as well as the total vertical displacements of top and bottom boundaries for Group-1 (with different vertical grouting positions). Labels A and B represent grouting taking place on A side (A1) and B side (B1), respectively, and the 0 m-elevation is at the bottom of the tunnel.

The curves show that the responses to the change of the grouting elevation are almost the same from two different sides (A1 and B1). An apparent turning point can be identified at 2.7 m, which is close to the middle elevation of the tunnel profile. When the grouting elevation is lower than this value, the horizontal displacements of the linings are insensitive to the change of the grouting elevation. The tunnel tends to move downwards as the elevation increases. An obvious reduction in the deformation is observed after the start point of the grouting is higher than the middle section of the ring. Fig.13b**Error! Reference source not found.** shows the recovery of convergence in two directions of the first group (the "dhc" and "dvc" are the increments of horizontal and vertical convergence of the left tunnel, respectively, with the negative value representing the reduction). To illustrate the deformed shape of the tunnel lining more clearly, the distortion degree (α) is added in Fig.13b, which indicates the position in the circumferential direction of the maximum tunnel deformation with respect to the horizontal axis, with a positive value representing a clockwise rotation. The distortion degrees are close to 0 for h2~h3; hence an efficient convergence recovery can be obtained when the start point of grouting is below 2.7 m, whereas it will get an obvious rotation when it comes to h1. This adverse rotation caused by the change of the loading direction is the primary reason for the appearance of the turning point. Similar conclusions can also be seen in other researches (Lueprasert et al., 2015; Lueprasert et al., 2017). The results here confirm that the

start point of grouting should not be higher than the middle of the tunnel to obtain a more efficient reduction of convergence.

Fig.13c presents the total displacement results for Group-2 with different horizontal grouting positions. Interestingly, the maximum deformation caused by grouting does not occur when the grouting position is closest to the tunnel (Case-12 and Case-16), but it occurs in correspondence with the original design (Case-5 and Case-17). A specific thickness of soil should remain between the lining and the grouting position to facilitate a more uniform transfer of the grouting pressure to the lining rings. Fig.13**Error! Reference source not found.**d also suggests the same critical distance for an efficient grouting treatment.

4.2 Grouting height

In Section 3, we have investigated the responses for two different heights of grouting zone, namely 5.2 m and 4.2 m. Here we add two further heights to provide a more complete picture of the effect of the grouting height, as listed in Table 5. The Case-3 from the experiment is set as the benchmark in this section and used to define other grouting parameters except for the height.

Table 5 Grouting parameters for sensitivity analysis of grout height

Case-Num	Grouting height / m	Grouting pipe	Case-Num	Grouting height / m	Grouting pipe
20	3.2	A2	23	3.2	B1
3	4.2	A2	24	4.2	B1
21	5.2	A2	25	5.2	B1
22	6.2	A2	26	6.2	B1

As the total volume is kept constant, the grouting volume per unit height decreases as the total height increases, and the grouting effect is expected to weaken due to an increasing size of the influence zone. Fig.14 shows the total displacement and recovery of convergence results. There appears to be a critical value for the grouting height in terms of the effect on the reduction of the convergence, and in the cases considered here the critical height is about 4.2 m, and with this height, the grouting zone is all located within the range of the tunnel height. When the grouting height is lower than 4.2m, an increase in the grouting height results in a more sensitive reduction of the convergence.

4.3 Grouting volume

The total grouting volume is one of the most important parameters and can be controlled easily in the operation to obtain the desired effect. Case-4 from the experiment is chosen as the benchmark in the parametric study on the effect of the grouting volume as it has the originally designed grouting elevation and height, and the details are presented in Table.6

Table.6 Grouting parameters of analysis on grouting positions

Case-Num	Initial particle's volume / V_p (m^3)	Grouting pipe	Case-Num	Initial volume / V_p (m^3)	Grouting pipe
27	0.10	A2	31	0.10	B1
28	0.15	A2	4	0.1441	B1
29	0.20	A2	32	0.20	B1
30	0.25	A2	33	0.25	B1

Fig.15 shows the results from variable grouting volume conditions. It can be observed that increasing grout volume leads to an increased reduction of the deformation, in terms of both the total displacements and the convergence, and the trend is approximately linear. There is a limit to the effectiveness by injecting more grout, and in the cases analyzed limiting volume is about 0.2 m^3.

5 Conclusions

The effect of grouting treatment in the recovery of excessive convergence of a metro shield tunnel located in soft ground area is studied using data from the field grouting experiment and numerical simulation with the MPM technique. The monitoring data of the convergence deformation of the tunnel linings provided detailed information allowing an analysis of the grouting effect under different situations with varying grout positions, grout volumes, and heights. On the other hand, a numerical modeling framework based on MPM is established. The numerical model is capable of replicating the grouting process in the soil explicitly, and thus enabling detailed examination into the convergence reduction effects of the grouting operation and the key influencing parameters.

The numerical model based on MPM is validated by comparison with the monitoring results. The results indicate that increasing the grouting height and volume within a limited range can improve its effect on the recovery of the tunnel's convergence, and the relative position of the grouting to the tunnel also influence the grouting efficiency. The numerical work gives the possibility of optimizing the design demonstrated by a sensitivity analysis.

References

[1] Artola, J., 2005. A solution to the braced excavation collapse in Singapore. Ph.D. thesis. Massachusetts Institute of Technology. https://dspace.mit.edu/bitstream/handle/1721.1/31123/61163849-MIT.pdf?sequence=2

[2] Azúa-González , C., Pozo, C., Askarinejad, A., 2018. Finite element analysis of soft boundary effects on the behaviour of shallow foundations. Numerical Methods in Geotechnical Engineering IX, Volume 2: Proceedings of the 9th European Conference on Numerical Methods in Geotechnical Engineering, Porto, Portugal. https://www.researchgate.net/profile/Carlos-Xavier-Azua-Gonzalez/publication/326106997_Finite_Element_analysis_of_soft_boundary_effects_on_the_behaviour_of_shallow_foundations/links/5b395be9a6fdcc8506e71496/Finite-Element-

analysis-of-soft-boundary-effects-on-the-behaviour-of-shallow-foundations.pdf

[3] Banthia, N., 2013. Fiber reinforced polymers in concrete construction and advanced repair technologies. Department of Civil Engineering University of British Columbia, 37. http://www.geosynthetica.com/Uploads/NBanthia15Dec.pdf

[4] Bezuijen, A., Talmon, A., Kaalberg, F.J., Plugge, R., 2004. Field measurements of grout pressures during tunnelling of the sophia rail tunnel. Soils and Foundations 44, 39-48. https://doi.org/10.3208/sandf.44.39

[5] Bolton, M., Lu, Y., Sharma, J., 1996. Centrifuge models of tunnel construction and compensation grouting. Proceedings of the International Symposium on Geotechnical Aspects of Underground Construction in Soft Ground, 471-476. http://publications.eng.cam.ac.uk/330807/

[6] Cheng, X., Zheng, G., Soga, K., Bandara, S., Kumar, K., Diao, Y., Xu, J., 2015. Post-failure behavior of tunnel heading collapse by MPM simulation. Science China Technological Sciences 58, 2139-2152. https://doi.org/10.1007/s11431-015-5874-4

[7] Ding, L., Xu, J., 2017. A review of metro construction in china: Organization, market, cost, safety and schedule. Frontiers of Engineering Management 4, 4-19. http://en.cnki.com.cn/Article_en/CJFDTOTAL-FOEM201701002.htm

[8] Ding, W., Duan, C., Zhu, Y., Zhao, T., Huang, D., Li, P., 2019. The behavior of synchronous grouting in a quasi-rectangular shield tunnel based on a large visualized model test. Tunnelling and Underground Space Technology 83, 409-424. https://doi.org/10.1016/j.tust.2018.10.006

[9] Fern, E., 2019. Modelling tunnel-induced deformations with the material point method. Computers and Geotechnics 111, 202-208. https://doi.org/10.1016/j.compgeo.2019.03.017

[10] Harris, D., Mair, R., Love, J., Taylor, R., Henderson, T., 1994. Observations of ground and structure movements for compensation grouting during tunnel construction at waterloo station. Geotechnique 44, 691-713. https://doi.org/10.1680/geot.1994.44.4.691

[11] Hu, Z., Yue, Z., Zhou, J., Tham, L., 2003. Design and construction of a deep excavation in soft soils adjacent to the shanghai metro tunnels. Canadian Geotechnical Journal 40, 933-948. https://doi.org/10.1139/t03-041

[12] Huang, H., Xiao, L., Zhang, D., Zhang, J., 2017. Influence of spatial variability of soil young's modulus on tunnel convergence in soft soils. Engineering Geology 228, 357-370. https://doi.org/10.1016/j.enggeo.2017.09.011

[13] Kasper, T., Meschke, G., 2006. A numerical study of the effect of soil and grout material properties and cover depth in shield tunnelling. Computers and Geotechnics 33, 234-247. https://doi.org/10.1016/j.compgeo.2006.04.004

[14] Katebi, H., Rezaei, A., Hajialilue-Bonab, M., Tarifard, A., 2015. Assessment the influence of

ground stratification, tunnel and surface buildings specifications on shield tunnel lining loads (by fem). Tunnelling and Underground Space Technology 49, 67-78. https://doi.org/10.1016/j.tust.2015.04.004

[15] Kiriyama, K., Kakizaki, M., Takabayashi, T., Hirosawa, N., Takeuchi, T., Hajohta, H., Yano, Y., Imafuku, K., 2005. Structure and construction examples of tunnel reinforcement method using thin steel panels. Nippon Steel Technical Report 92, 45-50. https://www.researchgate.net/publication/283863258_Structure_and_construction_examples_of_tunnel_reinforcement_method_using_thin_steel_panels

[16] Lambrughi, A., Rodr´ıguez, L., Castellanza, R., 2012. Development and validation of a 3d numerical model for tbm{epb mechanised excavations. Computers and Geotechnics 40, 97-113. https://doi.org/10.1016/j.compgeo.2011.10.004

[17] Li, X., Cao, W., Tao, M., Zhou, Z., Chen, Z., 2016. Influence of unloading disturbance on adjacent tunnels. International Journal of Rock Mechanics and Mining Sciences 84, 10-24. https://www.nipponsteel.com/en/tech/report/nsc/pdf/n9209.pdf

[18] Liao, S., Liu, J., Wang, R., Li, Z., 2009. Shield tunneling and environment protection in shanghai soft ground. Tunnelling and Underground Space Technology 24, 454-465. https://doi.org/10.1016/j.tust.2008.12.005

[19] Liu, J., Song, J., Zhang, Z., Hu, N., 2017. Influence of the ground displacement and deformation of soil around a tunnel caused by shield backfilled grouting during construction. Journal of Performance of Constructed Facilities 31. https://doi.org/10.1061/(ASCE)CF.1943-5509.0000989

[20] Lueprasert, P., Jongpradist, P., Charoenpak, K., Chaipanna, P., Suwansawat, S., 2015. Three dimensional finite element analysis for preliminary establishment of tunnel influence zone subject to pile loading. Maejo International Journal of ence and Technology, 209-223. https://doi.org/10.14456/mijst.2015.16

[21] Lueprasert, P., Jongpradist, P., Jongpradist, P., Suwansawat, S., 2017. Numerical investigation of tunnel deformation due to adjacent loaded pile and pile-soil-tunnel interaction. Tunnelling and Underground Space Technology 70, 166-181. https://doi.org/10.1016/j.tust.2017.08.006

[22] Mair, R., Hight, D., 1993. Report on session 4: displacement. http://publications.eng.cam.ac.uk/331624/

[23] MOHURD, 2014. Code for monitoring measurement of urban rail transit engineering (GB50911-2013). http://www.nssi.org.cn/nssi/front/83513840.html

[24] Nguyen, V., 2014. Material point method: basics and applications. Cardiff University, Department of Civil Engineering. https://www.researchgate.net/profile/Vinh_Phu_Nguyen/publication/262415477_Material_point_method_basics_and_applications/links/00463537ab99f084f0000000/Material-point-method-basics-and-applications.pdf

[25] Oh, J., Ziegler, M., 2014. Investigation on influence of tail void grouting on the surface settlements during shield tunneling using a stress-pore pressure coupled analysis. KSCE Journal of Civil Engineering 18, 803-811. https://doi.org/10.1007/s12205-014-1383-8

[26] Richefeu, V., Villard, P., 2016. Modeling gravity hazards from rockfalls to landslides. https://books.google.com/books?hl=zh-CN&lr=&id=k3iLCwAAQBAJ&oi=fnd&pg=PP1&ots=ag3zjkjvpG&sig=GXyPasLSCSdTcBlB7hPXAy3FsQw#v=onepage&q&f=false

[27] Soga, K., Bolton, M., Au, S., Komiya, K., Hamelin, J., Van Cotthem, A., Buchet, G., Michel, J., 1999. Development of compensation grouting modelling and control system, in: Proceedings of the International Symposium on Geotechnical Aspects of Underground Construction in Soft Ground, 19-21. http://publications.eng.cam.ac.uk/329896/

[28] Sulsky, D., Chen, Z., Schreyer, H., 1994. A particle method for history dependent materials. Computer Methods in Applied Mechanics and Engineering 118, 179-196. https://doi.org/10.1016/0045-7825(94)90112-0

[29] Wang, B., Hicks, M., Vardon, P., 2016. Slope failure analysis using the random material point method. Geotechnique Letters 6, 113-118. https://doi.org/10.1680/jgele.16.00019

[30] Wang, R., 2009. Factors influencing deformation of shanghai soft soil metro tunnel and deformation analysis. Underground Engineering and Tunnels 1, 1. http://en.cnki.com.cn/Article_en/CJFDTOTAL-DSGC200901000.htm

[31] Wisser, C., Augarde, C., Burd, H., 2005. Numerical modelling of compensation grouting above shallow tunnels. International Journal for Numerical and Analytical Methods in Geomechanics 29, 443-471. https://doi.org/10.1002/nag.421

[32] Woo, S., Salgado, R., 2018. Simulation of penetration of a foundation element in Tresca soil using the generalized interpolation material point method (gimp). Computers and Geotechnics 94, 106-117. https://doi.org/10.1016/j.compgeo.2017.08.007

[33] Xie, X., Liu, Y., Huang, H., Du, J., Zhang, F., Liu, L., 2007. Evaluation of grout behind the lining of shield tunnels using ground-penetrating radar in the Shanghai metro line, china. Journal of Geophysics and Engineering 4, 253-261. https://doi.org/10.1088/1742-2132/4/3/S03

[34] Ye, F., Zhu, H., He, C., 2009. Back-filled grouts diffusion model and its pressure to segments of shield tunnel. Rock and Soil Mechanics 30, 1307-1312. http://en.cnki.com.cn/Article_en/CJFDTOTAL-YTLX200905022.htm

[35] Zhang, D., Huang, Z., Wang, R., Yan, J., Zhang, J., 2018. Grouting based treatment of tunnel settlement: practice in shanghai. Tunnelling and Underground Space Technology 80, 181-196. https://doi.org/10.1016/j.tust.2018.06.017

[36] Zhang, F., Xie, X., Huang, H., 2010. Application of ground penetrating radar in grouting evaluation for shield tunnel construction. Tunnelling and Underground Space Technology 25, 99-107. https://doi.org/10.1016/j.tust.2009.09.006

[37] Zhao, T., Ding, W., Qiao, Y., Duan, C., 2019. A large-scale synchronous grouting test for a quasi-rectangular shield tunnel: Observation, analysis and interpretation. Tunnelling and

Underground Space Technology 91, 103018.1-103018.18.
https://doi.org/10.1016/j.tust.2019.103018

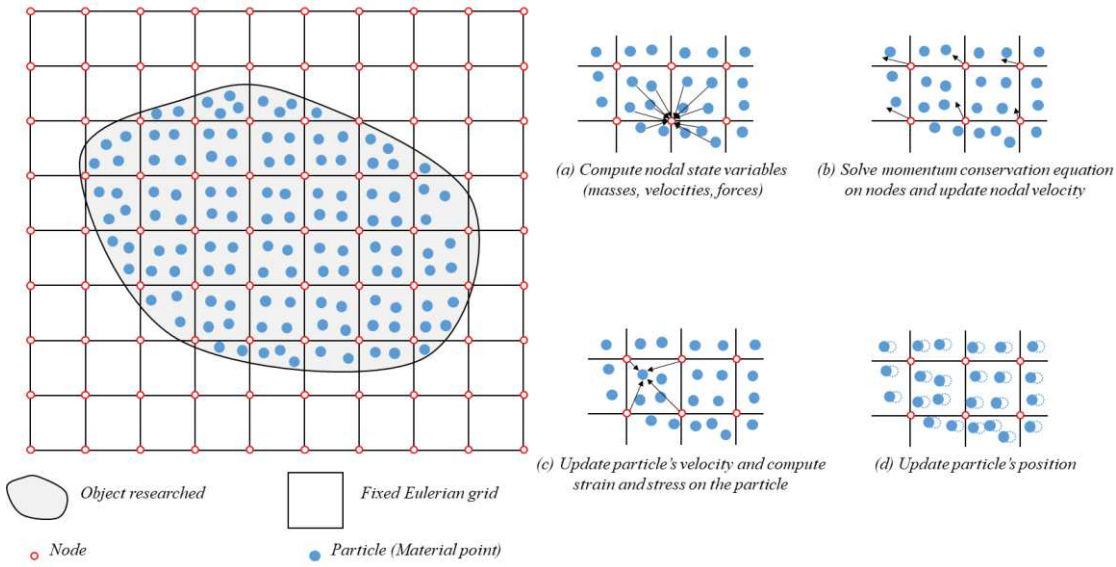

Fig.1 Illustration of the material point method

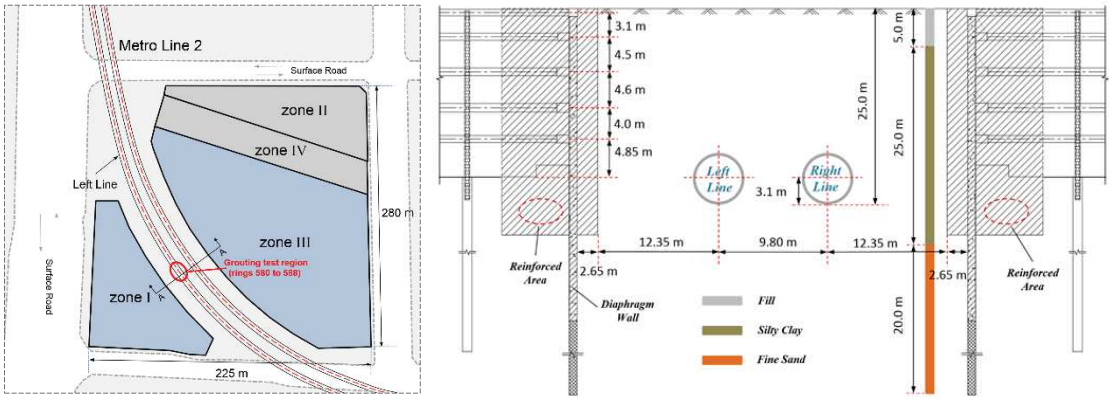

(a) **(b)**

Fig.2 Excavation zone and existed tunnels: (a)Plain view, (b)Side view

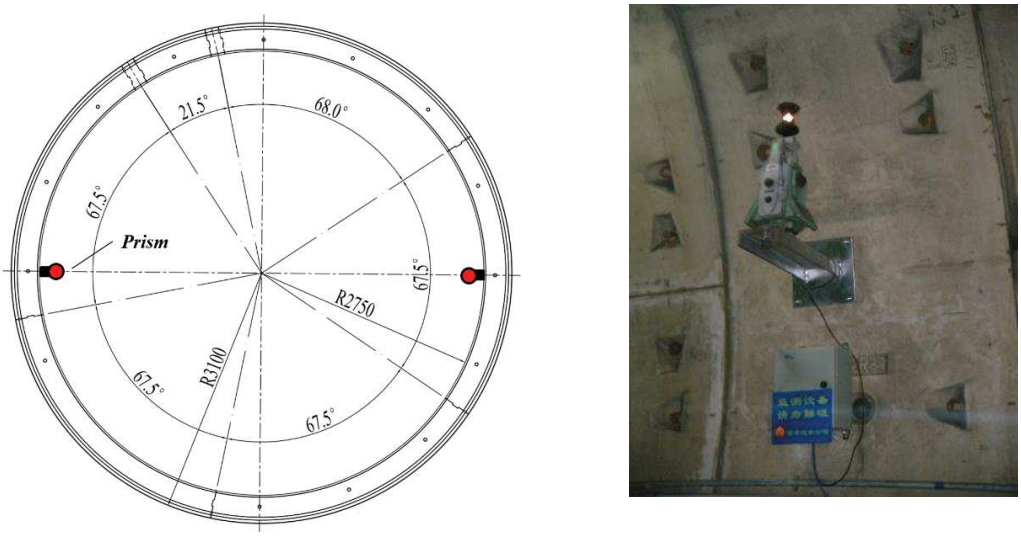

(a) (b)

Fig.3 Lining ring structure: (a)Segments, (b)Robotic total station

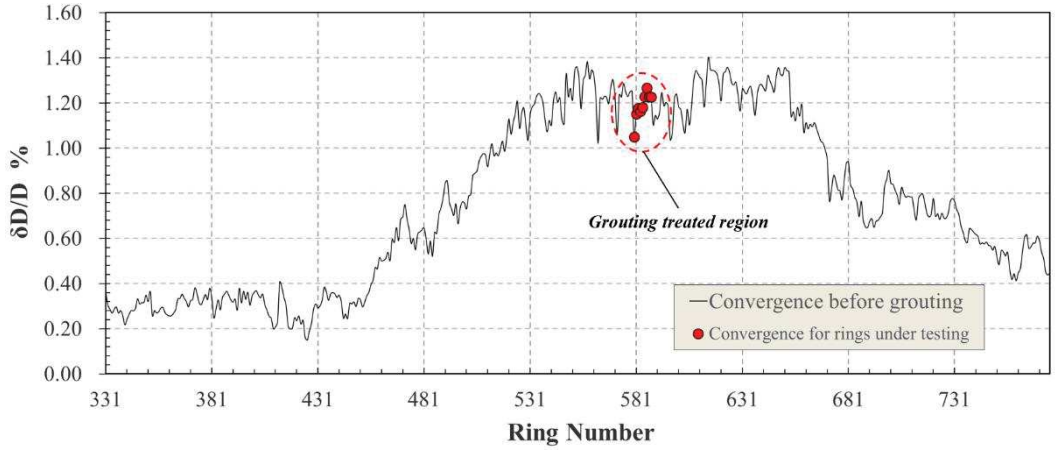

Fig.4 Convergence distribution before grouting (left line)

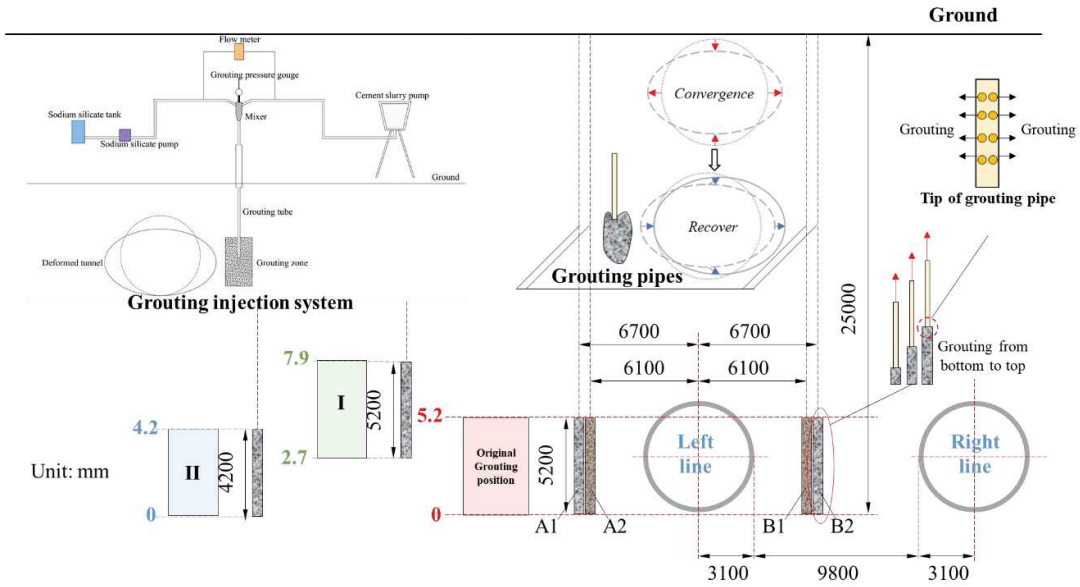

Fig.5 Geometry of the grouting work

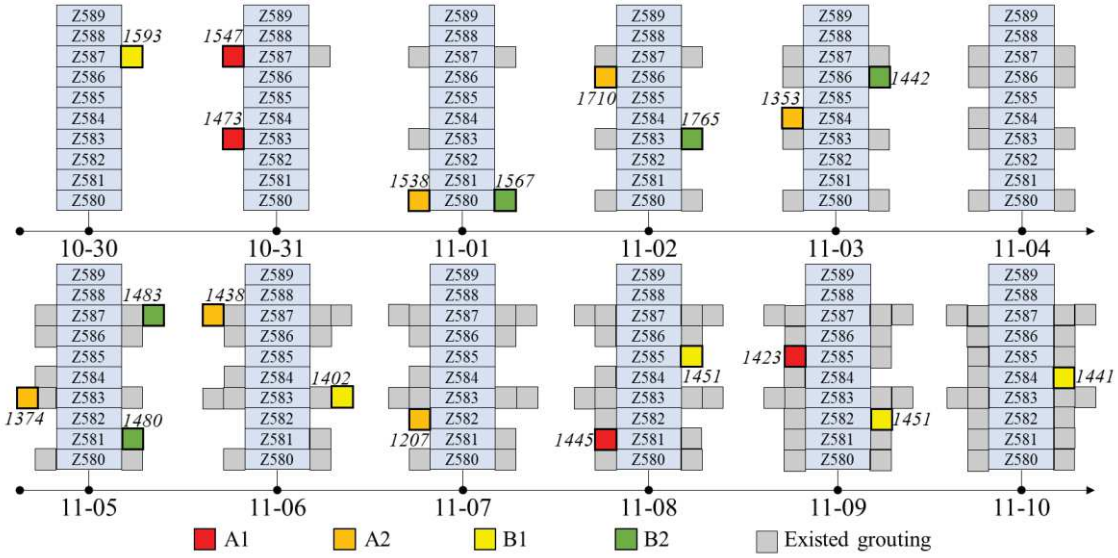

Fig.6 Grouting experiment schedule

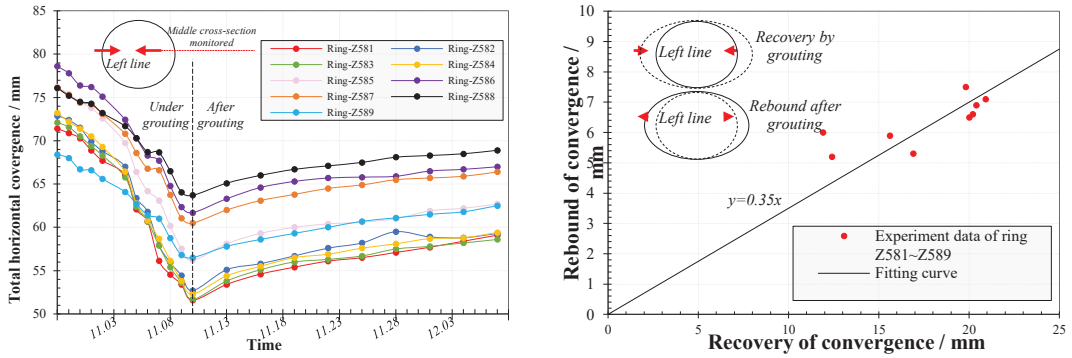

(a) (b)

Fig.7 Evolutions of lining's convergence: (a) Total convergence, (b)Relationship between the recovery and rebound values

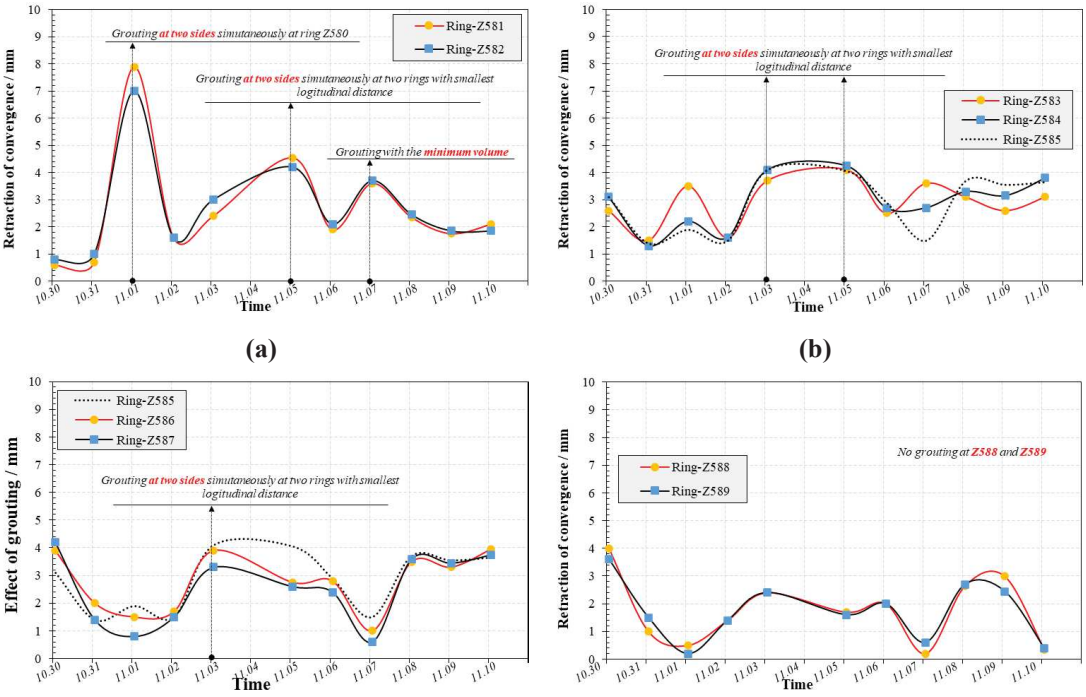

(a) (b)

(c) (d)

Fig.8 Recovery of convergence by grouting in the experiment: (a)Ring-Z581~Z582, (b)Ring-Z583~Z585, (c)Ring-Z585~Z587, (d)Ring-Z588~Z589

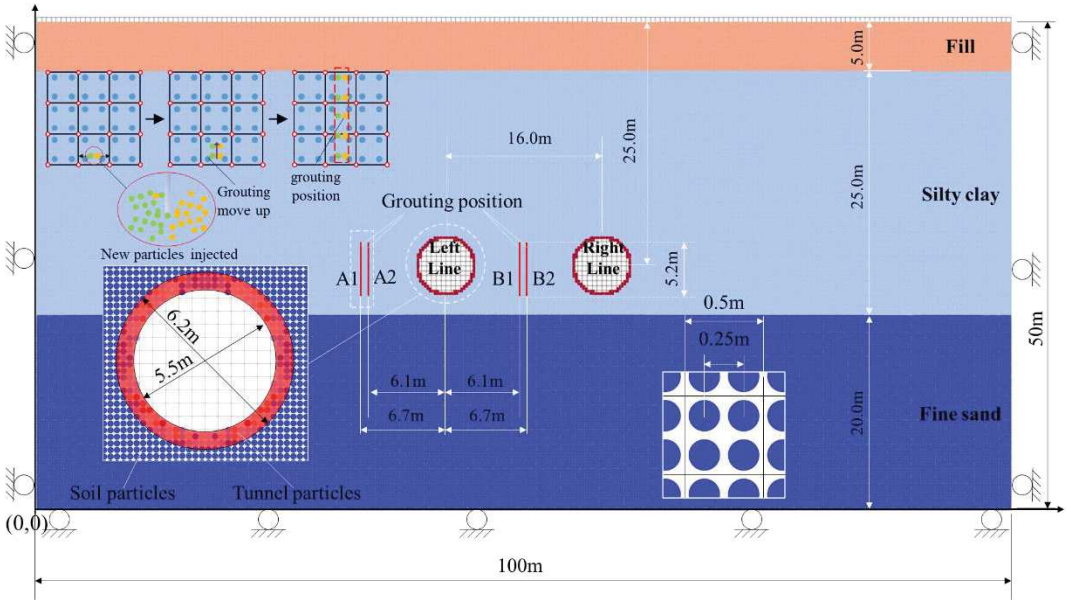

Fig.9 General information of the MPM model

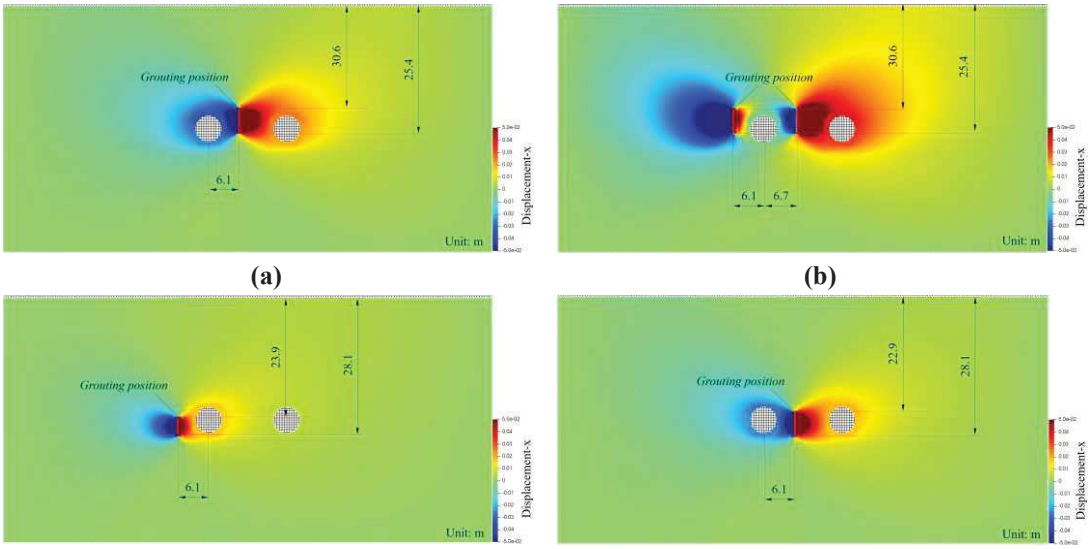

Fig.10 Contours of excessive x-displacement by grouting: (a)Case-1, (b)Case-2, (c)Case-3, (d)Case-4

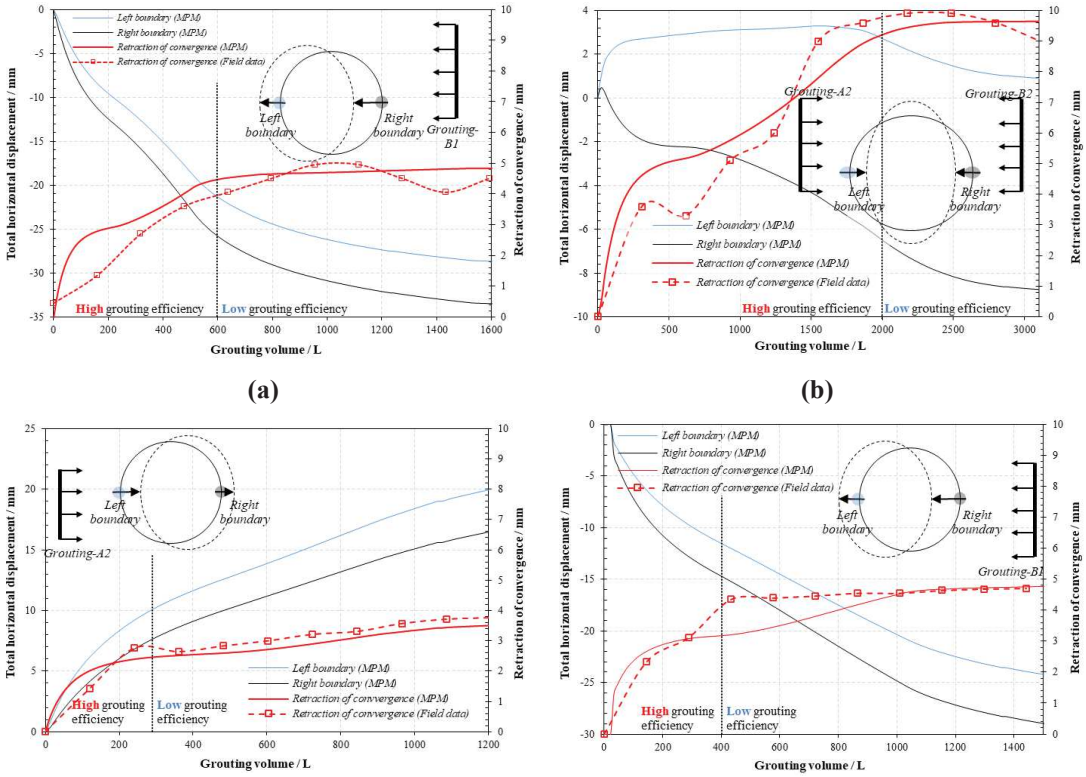

Fig.11 Recovery of convergence by grouting in the MPM model: (a)Case-1, (b)Case-2, (c)Case-3, (d)Case-4

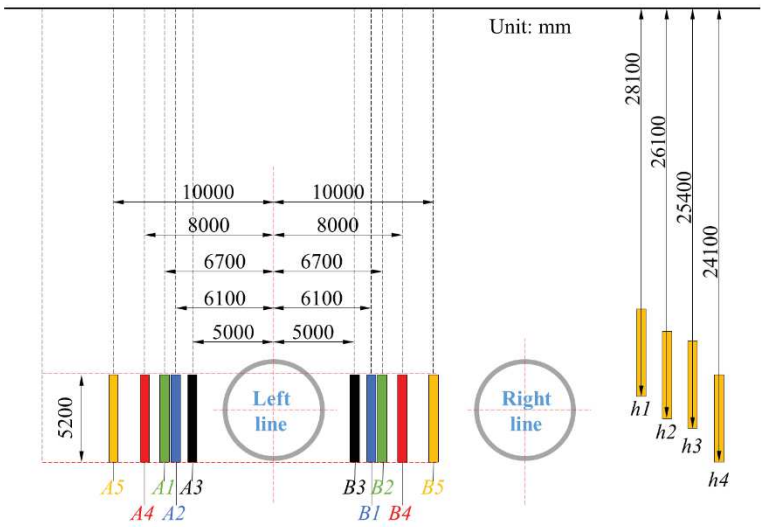

Fig.12 Grouting zone of different cases

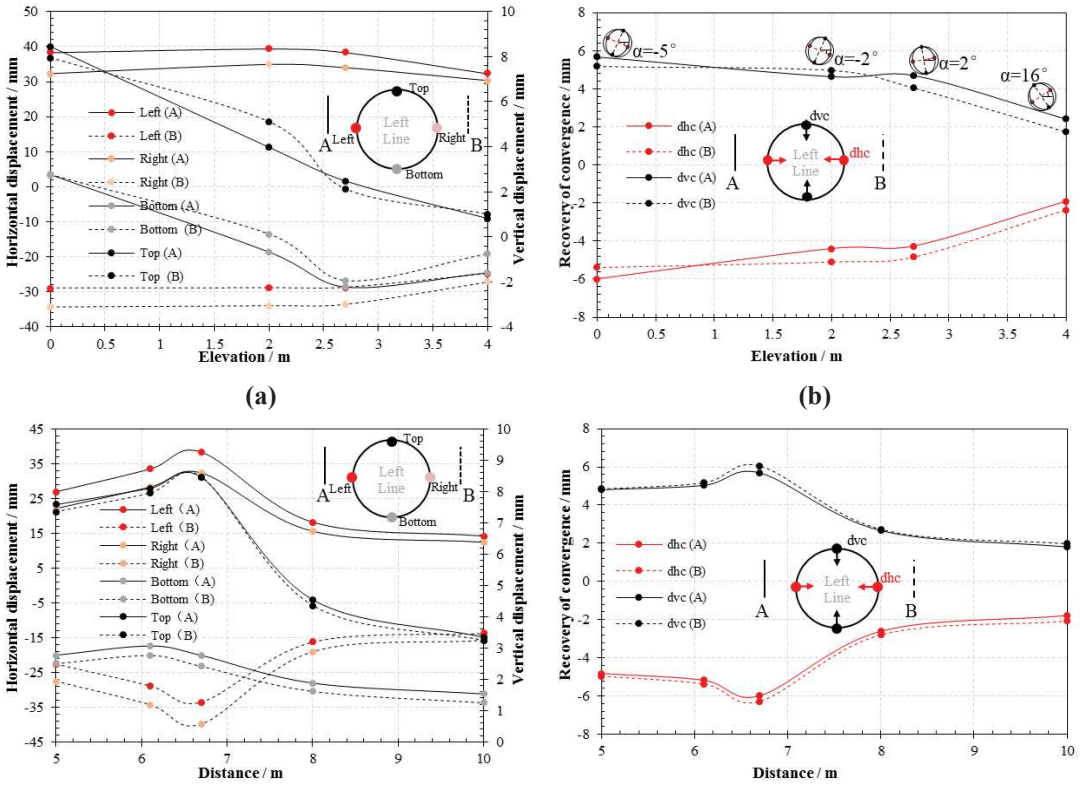

Fig.13 Displacements with different grouting positions: (a)Total displacement with different vertical position, (b)Recovery of convergence with different vertical position, (c)Total displacement with different horizontal position, (d)Recovery of convergence with different horizontal position

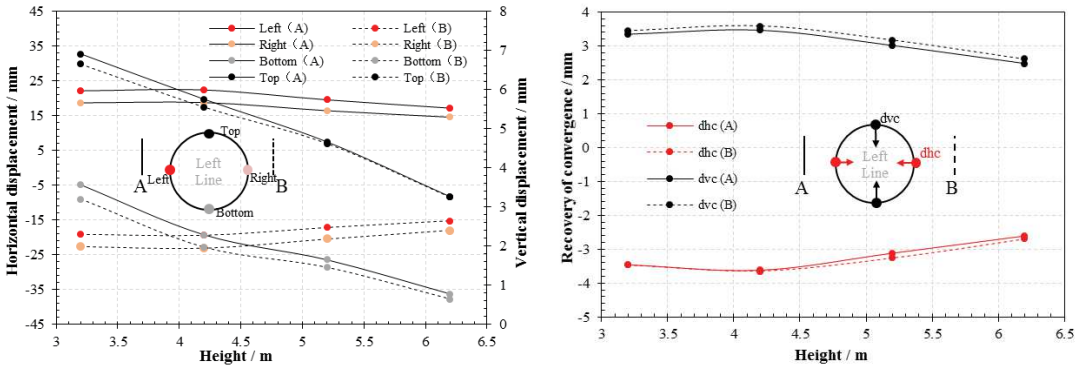

Fig.14 Displacements with different grouting heights: (a)Total displacement, (b)Recovery of convergence

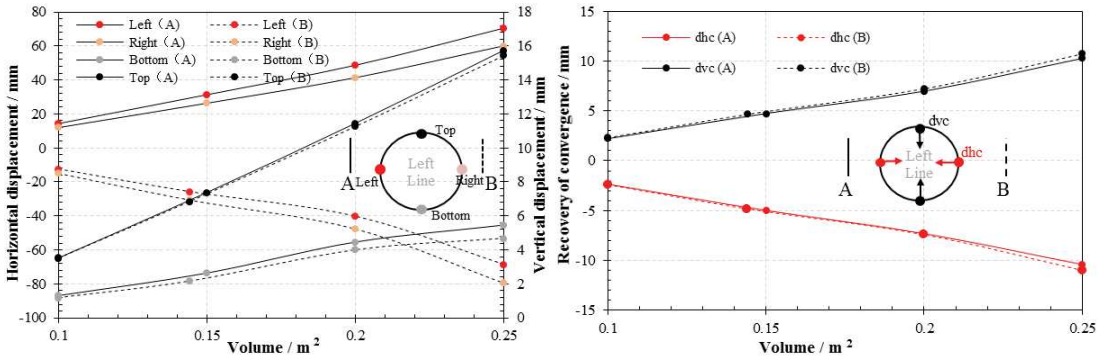

(a) (b)

Fig.15 Displacements with different grouting volumes: (a)Total displacement, (b)Recovery of convergence